Fiber-Coupled Microcavity Probe for in Vivo Near-Field Sensing

Zachary Ballard, Nichaluk Leartprapun, Jimmy Xu
School of Engineering
Brown University
Providence, USA
e-mail: Zachary_Ballard@brown.edu,
Nichaluk_Leartprapun@brown.edu,
Jimmy_Xu@brown.edu

Jimmy Xu
WCU Program
Seoul National University
Seoul, South Korea
e-mail: Jimmy_Xu@brown.edu

***Abstract*— We report on a new design for near-field sensing based on a fiber-coupled microcavity. The device operates on the bases of sensing in the evanescent near-field zone and offers a robust portable probe solution for in-vivo sensing and diagnostics. In preliminary tests, the first generation device has already demonstrated sensitivity in the range of 10^{-3} and 10^{-4} refractive index units (RIU) and 20 nm/RIU. Using this device, we have also observed, through spectral shift, the binding of a self-assembled monolayer (~ 5 Å thickness) of amino-silane.**

Keywords-Biosensor; Microprobe; microcavity

I. INTRODUCTION

The proliferation of optical bio-sensors has made point of use diagnostics a reality. Label free bio-sensors interact with biological materials often times in bulk solution without the need for any fluorescent bio-markers or dyes, allowing for a more elegant detection or diagnostic protocol [1].

Though many breakthroughs have been made in regard to detection sensitivity, bringing this technology from a lab (optical table) setting into a scalable and robust micro-device remains a challenging problem [2]. Furthermore, there exists a demand for in-vivo or in-situ use for real-time monitoring of cellular environments. Fiber-optic based platforms with sub-micron sized dimensions prove to be one of the more promising technologies due to their needle-like geometries [3]. Despite the functional advantages and published sensitivities around 10^{-4} to 10^{-7} RIU, optical fiber based platforms still remain several orders of magnitude less sensitive than other bio-sensing technologies such as Surface Plasmon Resonance sensors, Whispering Gallery Mode sensors, and interferometric sensors [4]. However, novel fiber-based platforms could increase the capacity for sensitivity and serve as a more robust and low-cost bio-sensor solution. A portable high-sensitivity in-vivo device could have immense impact in driving down the cost of healthcare and guiding vaccine and medicinal distribution networks [5].

This work-in-progress report presents a novel bio-sensor with a probe structure that has the potential for in-vivo or in-situ sensing and probing of bio-environments. This simple, portable, micro-scale device can pick up minute changes, via phase-shift and amplitude change, in its microcavity's immediate vicinity (evanescence zone). It could be used for diagnostics or deoxyribonucleic acid (DNA) and protein assays, and as a possible low-cost tool to aid in the understanding of binding events of specific target molecules. The micro-probe consists of a micro-cavity formed at, and optically coupled to, the tip of an optical fiber, resulting in a compact, simple, and bio-compatible design for refractive index sensing. Preliminary experiments for the first generation device have yielded an initial, non-optimized limit of detection of 10^{-3} to 10^{-4} RIU with 20 nm/RIU.

This manuscript will discuss the fabrication and structure of the fiber-coupled micro-cavity probe, the working principles, and provide experimental validations and preliminary detection capabilities

II. DEVICE DESCRIPTION

The micro-probe is made by tapering hollow borosillicate tubes (1mm OD, .75 mm ID) down to tip diameters of 25-50 µm. The tapering was achieved using a Sutter Instrument P-2000 Micropipette Puller. A 20W Class IV CO_2 laser was used as the heating source while the borosilicate tube was pulled from both sides as shown in Fig. 1. Custom programs were written for the pipette puller to achieve long and gradual tapers. The tapered tips were then melted with a gentle flame from standard butane lighter, whereupon the molten glass forms a solid glass spherical tip due to surface tension. The symmetry of the spherical tips was maintained by constant spinning of the tips during the melting process. The total resulting structure consists of a finely tapered air cavity that extends into a solid glass spherical tip, as seen in Fig. 2.

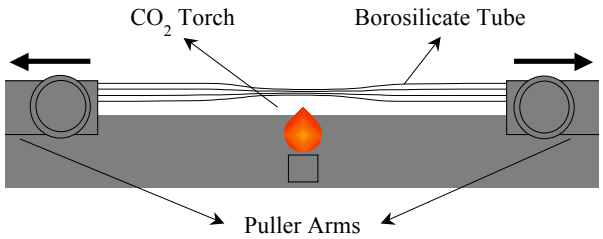

Figure 1. Borosilicate tube tapering process using a Micropipette Puller

Then, standard SMF-28 telecom fibers were stripped, cleaved and inserted into this tapered cavity, eventually becoming wedged. The optical fiber remains stationary due to the cylindrical geometry of the tapered air cavity and

 ISBN: 978-1-61208-297-4

fiber, and can be affixed upon its insertion point with simple epoxy.

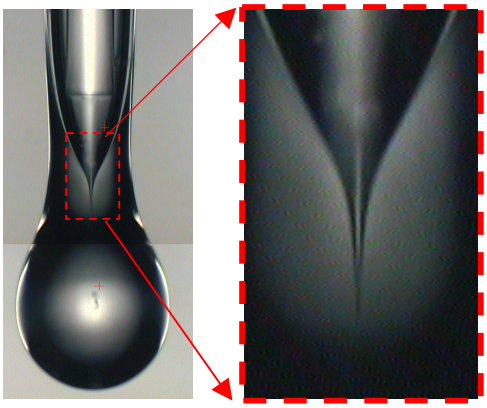

Figure 2. Device structure: (a) SMF-28 fiber (125 μm diameter) wedged in tapered air cavity (410 μm diameter) and (b) tapered air cavity.

The range of spherical tip diameters tested so far were, but not limited to, 300-500 microns.

III. WORKING PRINCIPLES

A. *Fizeau Interferometry*

The resulting spherical probe structure contains two effective reflection surfaces for incident light through the optical fiber [6]. The first interface is between the end of the cleaved fiber and the air cavity, and the second interface is between the edge of the solid glass spherical tip and the outside environment, as shown in Fig. 3. Therefore, when incoming light through the fiber enters the device, the reflection from the second interface recombines with the reflection from the first interface described by the reflection from an effective Fabry-Perot cavity.

The second interface is an effective one that is subjected to change by the material in the evanescence-zone of the probe tip. The spherical tip forms a secondary (weak Q) cavity for the entering light scattered from the sharp air-tip.

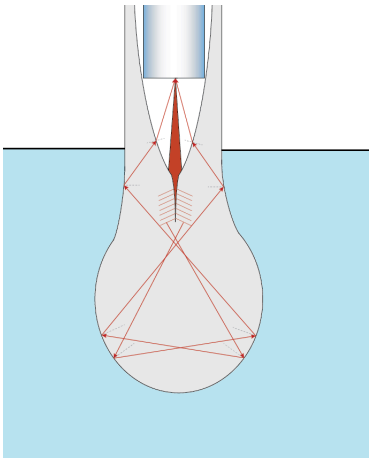

Figure 3. Ray-optics of light propagation in probe geometry.

Surrounding the outer surface of this microcavity is the aforementioned evanescence-zone. A change of material, temperature, or pH, even a minute one, in this zone would effectively change the size of this cavity, which translates into a phase-shift that can be measured from the overall interference pattern.

B. *Use as a Sensor*

Increasing the refractive index of the environment outside of the spherical tip naturally decreases the reflection coefficient for reflections below the critical angle and thus decreases the amplitude of the interference signal. However, this is not the only effect. Experiments show a clear phase change with changing refractive index in exterior environments.

Due to the unique geometry of the sharply tapered air cavity between the two reflection interfaces, this device is able to bend the wave fronts of the fiber-outputted light in such a way that allows for multiple reflections in the spherical silica tip and probe neck, eventually coupling the light back into the optical fiber. This light propagates in the spherical tip with a refractive index, n_1, through a series of reflections with non-normal incident angle, θ_i, allowing the reflections which meet the total internal reflection criteria are greatly affected by the Goos-Hänchen effect [7]. Changing the refractive index, n_2, at the interface along the spherical tip will modulate the Goos-Hänchen shift, thus, shifting the interference pattern by a phase, δ, described by,

$$\tan\left(\frac{\delta_S}{2}\right) = \frac{\left(\sin\theta_i{}^2 - n^2\right)^{\frac{1}{2}}}{\cos\theta_i} \quad (1a)$$

$$\tan\left(\frac{\delta_P}{2}\right) = \frac{\left(\sin\theta_i{}^2 - n^2\right)^{\frac{1}{2}}}{n\cos\theta_i} \quad (1b)$$

where $n = n_2/n_1$.

Treating the device as an effective Fabry-Perot cavity [6], the total reflected intensity could be derived using the Airy Summation Method,

$$I_r(FP) = I_0\left[\frac{r_1^2 + 2\cos(\delta)r_1r_2 + r_2^2}{1 + 2\cos(\delta)r_1r_2 + r_1^2r_2^2}\right], \quad (2)$$

where r_1 and r_2 represent the reflection coefficient of the two interfaces of an asymmetric Fabry-Perot cavity. Substituting $r_1 = -r_2$ into (2) would recover the standard equation for the reflection of a symmetric Fabry-Perot cavity. Fig. 4 shows the model interference patterns produced from (2) for n_2 of air, water, and ethanol. The experimentally obtained interference patterns for the same environment are shown in Fig. 5.

 ISBN: 978-1-61208-297-4

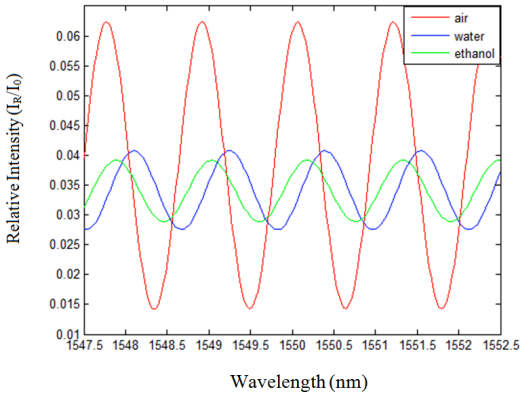

Figure 4. Output of probe model for outside refractive index environments of air, water, and ethanol.

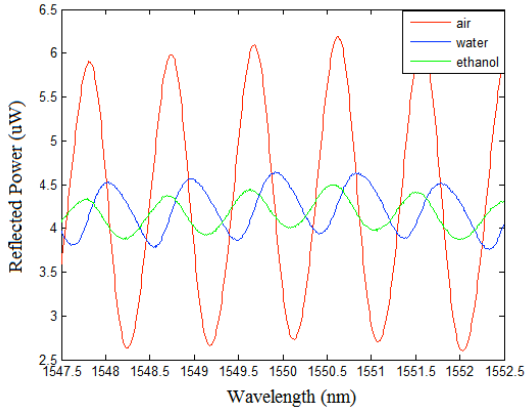

Figure 5. Reflected power (μW) measured for probe during 5 nm sweep in air, water, and ethanol.

This effective F-P model worked remarkably well, despite the complex structure and geometry, and can be used as a tool by which to measure material changes in the probe's immediate vicinity or specific binding events.

IV. EXPERIMENTAL DEMONSTRATION

A. Experimental Set-Up

The experimental set-up to demonstrate the interference properties of the fiber-coupled micro-sphere tip is illustrated in Fig. 6. An Ando AQ4320D Tunable Laser Source was wired to a 2×1 fiber optic coupler. The output of the coupler was sent to the SMF-28 fiber wedged in the micro-sphere tip. The reflected signal from the tip was measured by an Ando AQ6317 Optical Spectrum Analyzer wired to the second output of the coupler.

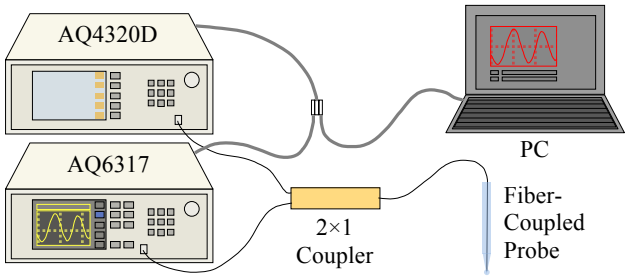

Figure 6. Experimental set-up for fiber-coupled micro-sphere tip interference measurements.

Both the Tunable Laser Source and the Optical Spectrum Analyzer were connected to a PC and controlled by a LabVIEW VI. Spectra collection was also accomplished by the same program.

B. Refractive Index Sensing with Ethanol-Water Mixture

For a quantitative assessment of the sensitivity of this device, the probe was submerged in 0.5 mL DI water and then subsequently submerged in incremental concentrations of ethanol-water mixtures ranging from 0 to 50% volume fraction of ethanol. In each mixture, a 3 nm spectral sweep was performed centered around 1550 nm with 1 mW laser power. The reflected power was measured and demonstrated a red spectral shift with increasing ethanol concentration, as shown in Fig. 7.

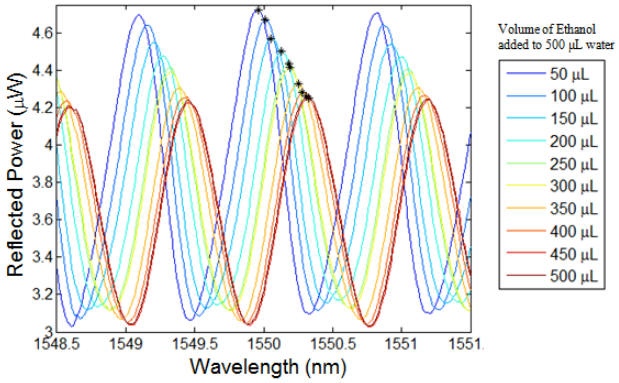

Figure 7. Blue to red shift of interference pattern show incremental 10^{-3} RIU changes in each measured ethanol-water mixture.

The refractive index of each ethanol-water mixture was measured using a Fisher Scientific Abbe Benchtop Refractometer. Fig. 8 plots the peak-to-peak amplitude of the spectrums and the peak wavelength as a function of mixture refractive index. Both the intensity change and spectral shift demonstrated a near-linear change with increasing refractive index, demonstrating a sensitivity of ~10^{-3} RIU, and 20 nm/RIU.

 ISBN: 978-1-61208-297-4

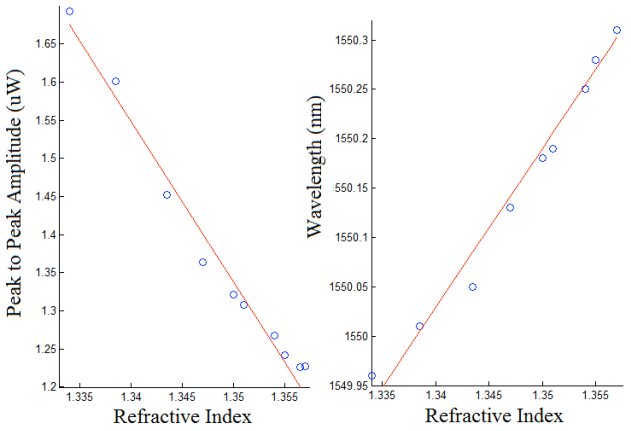

Figure 8. (a) Peak to peak amplitude of the measured interference and (b) the corresponding wavelength at each interference peak (spectral shift).

Deviations from the linearity could be due to temperature fluctuations during testing as well as non-uniform mixing in the ethanol-water samples. Further testing must be done in a flow-system for temperature and mixing control in order to experimentally demonstrate a higher Limit of Detection (LOD).

C. *Monitory Formation of Self-Assembled Monolayer*

The probe surfaces were cleaned in Piranha solution (3:1 v/v of H_2SO_4:H_2O_2) and then placed in a solution of 2% v/v of 3-aminopropyltriethoxysilane (APTES) in acetone [8]. The solution was sealed with a molded polydimethylsiloxane (PDMS) stopper and PTFE thread seal tape to avoid evaporation. Silanization of APTES refers to the binding of APTES molecules onto a substrate surface. It is often used to functionalize silica substrates for selective immobilization of protein bio-targets [9]. The probe was submerged in the solution for 12 hours as continuous 3 nm spectral sweeps, centered around 1550 nm with 1 mW laser power, were taken. The interference patterns obtained during the 12-hour APTES silanization exhibit blue spectral shift, as shown in Fig. 9.

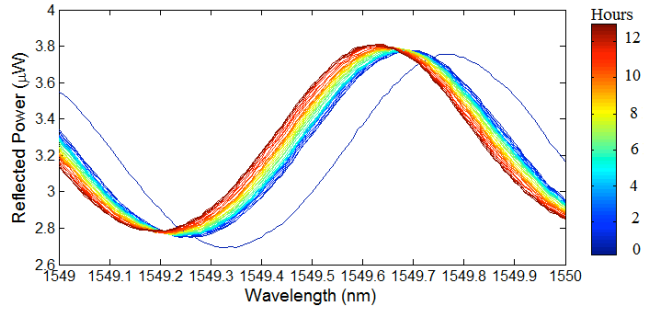

Figure 9. Spectral shift of interference pattern due to silanization during the first 12 hour of incubation.

This result is counter to the spectral shifts observed in typical resonance sensors, caused by an effective lengthening of the optical path due to the presence of the monolayer [10][11][12]. However, this counter-intuitive effect was reproduced in multiple molecular binding experiments, and could be caused by a lessening of optical tunneling into the bulk solution due to the higher Δn between the APTES layer and the bulk solution (assuming that $n_{APTES} > n_{Glass}$).

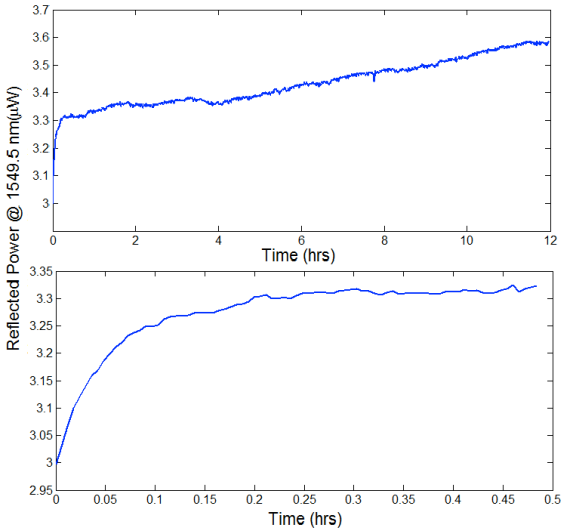

Figure 10. Reflected power at single wavelength during silanization process plotted at (a) the 12-hour incubation period and (b) during the first 30 minutes of incubation.

The reflected power change at 1549.5 nm (rising inflection point) of the interference pattern, shown in Fig. 10, illustrates the self-assembly of the APTES monolayer in the first 30 minutes, and subsequent intermolecular interactions of APTES molecules on top of this monolayer in the 12-hour period after the monolayer formation, resulting in a total spectral shift of ~0.2 nm. This observed monolayer binding time-scale (~30 minutes) agrees with the standard binding protocol time-scale for a 5 Å monolayer formation of APTES on a silica substrate [9].

V. CONCLUSION

Demonstrating the mode coupling between an optical fiber and microcavity sphere works to bring the high sensitivity of microcavity sensors, particularly Whispering Gallery Mode sensors, off of the optical table and into a robust integrated microprobe [13]. The probe design has the distinct advantage of use in vivo without the need of microfluidics or alignment of evanescent coupling, and can be implemented for sample volumes on the order of nano-liters. The first generation microprobes demonstrated sensitivity in the range of 10^{-3} and 10^{-4} RIU and 20 nm/RIU in bulk solutions. In addition, monitoring of the spectral shift during the salinization process confirms a high degree of near-field (evanescent) sensitivity due to immobilized surface molecules as the formation of the 5 Å self-

 ISBN: 978-1-61208-297-4

assembled APTES monolayer was detected in real-time. Thus, the experimental results demonstrates the proof-of-concept that this fiber-coupled microcavity probe can be used for detection of specific immobilized bio-targets, and even has potential use in studying real-time surface reaction kinetics.

Furthermore, though exhibiting sensitivity in bulk solution less than that achieved in other optical biosensors such as Surface Plasmon Resonance sensors, ring resonator sensors and interferometric sensors, which are able to detect down to 10^{-7} RIU, the data recorded thus far is from proof-of-concept hand-made microprobes that are yet to undergo optimization as far as their cavity size and geometric effects on mode coupling [4]. For example, by fabricating smaller diameter spherical tips, we will be able to increase the nm/RIU limit of detection due to a shorter effective cavity length. Similarly, implementing a controlled and mechanical method for melting and shaping the tapered tube, we hope to optimize the geometry of the tapered air cavity and probe curvatures. This optimization could lead to enhanced mode coupling between the fiber and the spherical tip. The geometric variations of the tapered air cavity and probe curvature could allow for tunability between the competing effects of the reflection coefficient modulation and Goos-Hänchen phase shift for the creation of far field and near field sensors respectively.

ACKNOWLEDGMENT

The authors wish to thank Anubhav Tripathi and Domenico Pacifici for their support and helpful discussion for this study. The authors are also very grateful for the guidance of Jin Ho Kim, Gustavo Fernandes, and Carlos Bledt, and the support of ARL, AFOSR, CR Bard Fellowship, and WCU.

REFERENCES

[1] M. A. Cooper, "Label-free screening of bio-molecular interactions."*Analytical and bioanalytical chemistry* 377.5, Nov. 2003, pp. 834-842, doi: 10.1007/s00216-003-2111-y.

[2] F. S. Ligler, "Perspective on optical biosensors and integrated sensor systems." *Analytical chemistry* 81.2, 2009, pp. 519-526, doi: 10.1021/ac8016289.

[3] M. N. Velasco-Garcia, "Optical biosensors for probing at the cellular level: A review of recent progress and future prospects." *Seminars in cell & developmental biology* 20.1. Academic Press, Feb. 2009, pp. 27-33, doi: 10.1016/j.semcdb.2009.01.013.

[4] X. Fan, I. M. White, S. I. Shopova, H. Zhu, J. D. Suter, and Y. Sun, "Sensitive optical biosensors for unlabeled targets: A review." *Analytica chimica acta* 620.1, Jul. 2008, pp. 8-26, doi: 10.1016/j.aca.2008.05.022.

[5] S. Rodriguez-Mozaz, M. J. Lopez de Alda, M. Marco, and D. Barcelo, "Biosensors for environmental monitoring: A global perspective." *Talanta* 65.2, Jan. 2005, pp. 291-297, doi: 10.1016/j.talanta.2004.07.006.

[6] O. R. Ranjbara, et al. "High pressure discrimination based on optical fiber microsphere cavity Fizeau interferometer." *Proc. of SPIE 8421*, Oct. 2012, doi: 10.1117/12.966322.

[7] D. Q. Chowdhury, D. H. Leach, and R. K. Chang, "Effect of the Goos-Häinchen shift on the geometrical-optics model for spherical-cavity mode spacing." *JOSA A* 11.3, 1994, pp. 1110-1116, doi: 10.1364/JOSAA.11.001110.

[8] A. V. Krasnoslobodtsev and S. N. Smirnov, "Effect of water on silanization of silica by trimethoxysilanes." *Langmuir* 18.8, 2002, pp. 3181-3184, doi: 10.1021/la015628h.

[9] M. Zhu, M. Z. Lerum, and W. Chen, "How to prepare reproducible, homogeneous, and hydrolytically stable aminosilane-derived layers on silica."*Langmuir* 28.1, 2012, pp. 416-423, doi: 10.1021/la203638g.

[10] F. Vollmer and S. Arnold, "Whispering-gallery-mode biosensing: label-free detection down to single molecules." *Nature methods* 5.7, Jul. 2008, pp. 591-596, doi: :10.1038/NMETH.1221.

[11] K. M. De Vos, I. Bartolozzi, P. Bienstman, R. Baets, and E. Schacht, "Optical biosensor based on silicon-on-insulator microring cavities for specific protein binding detection-art. no. 64470K." *Nanoscale Imaging, Spectroscopy, Sensing, and Actuation for Biomedical Applications IV* 6447, 2007, pp. 64470K1-64470K8, doi: 10.1117/12.698875.

[12] Y. Guo, et al. "Label-free biosensing using a photonic crystal structure in a total-internal-reflection geometry." *SPIE BiOS: Biomedical Optics* 7188, Feb. 2009, pp. 71880B–71880B12, doi: 10.1117/12.808369.

[13] S. Arnold, S. I. Shopova, and S. Holler, "Whispering gallery mode bio-sensor for label-free detection of single molecules: thermo-optic vs. reactive mechanism." *Optics Express* 18.1, Jan. 2010, pp. 281-287, doi: 10.1364/OE.18.000281.

 ISBN: 978-1-61208-297-4